Research Article

NGR-tagged nano-gold: A new CD13-selective carrier for cytokine delivery to tumors

Flavio Curnis[1] (✉), Martina Fiocchi[1], Angelina Sacchi[1], Alessandro Gori[2], Anna Gasparri[1], and Angelo Corti[1,3] (✉)

[1] *Division of Experimental Oncology, IRCCS San Raffaele Scientific Institute, Milan 20132, Italy*
[2] *Istituto di Chimica del Riconoscimento Molecolare, CNR, Milan 20131, Italy*
[3] *Vita Salute San Raffaele University, Milan 20132, Italy*

ABSTRACT

Colloidal gold (Au), a well-tolerated nanomaterial, is currently exploited for several applications in nanomedicine. We show that gold nanoparticles tagged with a novel tumor-homing peptide containing Asn-Gly-Arg (NGR), a ligand of CD13 expressed by the tumor neovasculature, can be exploited as carriers for cytokine delivery to tumors. Biochemical and functional studies showed that the NGR molecular scaffold/linker used for gold functionalization is critical for CD13 recognition. Using fibrosarcoma-bearing mice, NGR-tagged nanodrugs could deliver extremely low, yet pharmacologically active doses of tumor necrosis factor (TNF), an anticancer cytokine, to tumors with no evidence of toxicity. Mechanistic studies confirmed that CD13 targeting was a primary mechanism of drug delivery and excluded a major role of integrin targeting consequent to NGR deamidation, a degradation reaction that generates the isoAsp-Gly-Arg (isoDGR) integrin ligand. NGR-tagged gold nanoparticles can be used, in principle, as a novel platform for single- or multi-cytokine delivery to tumor endothelial cells for cancer therapy.

1 Introduction

The efficacy of cytokines in cancer therapy is often limited by their toxicity and counter-regulatory mechanisms. For example, the anti-tumor activity of tumor necrosis factor-alpha (TNF), an inflammatory cytokine with potent anti-tumor activity, is limited by a prohibitive systemic toxicity and by the release of soluble TNF-receptors into the circulation that inhibit its anticancer activity [1]. We have previously shown

that these limitations can be overcome, at least in the cases of TNF and interferon (IFN)-gamma, by administering extremely low amounts of cytokines fused to tumor vasculature-homing ligands, a strategy that enables "active" targeted delivery of pharmacologically relevant doses of cytokines to tumors [2–4]. One of these products, NGR-TNF, which consists of TNF fused to a tumor-homing disulfide-bridged peptide containing Asn-Gly-Arg (NGR), is now under investigation as an anticancer drug in phase II and III

Address correspondence to Flavio Curnis, curnis.flavio@hsr.it; Angelo Corti, corti.angelo@hsr.it

clinical studies, with evidence of activity and good tolerability [1, 2, 5–7].

The therapeutic index of cytokines can also be increased by an alternative strategy based on cytokine coupling with colloidal gold, a well-tolerated nanomaterial currently exploited for several applications in the field of nanomedicine [8, 9]. For example, the therapeutic index of TNF is significantly increased by coupling with 27-nm gold nanoparticles [10], a formulation that is being tested in cancer patients, with evidence of improved efficacy [11, 12]. The improved activity of nanogold-based drugs is likely dependent on "passive" targeting mechanisms owing to abnormally leaky vasculature in tumors, which leads to enhanced permeability and drug retention in neoplastic tissues [10].

The combination of "active" and "passive" targeting mechanisms might represent an efficient strategy for improving the delivery of cytokines to the tumor vasculature, thereby reducing the cytokine dose necessary to induce pharmacological effects and minimizing the activation of counter-regulatory mechanisms. This could be achieved, in principle, by coupling gold nanoparticles with tumor-homing ligands selective for receptors that are overexpressed by tumor cells and/or vasculature.

Disulfide-bridged NGR peptides (e.g., CNGRC) could be exploited for this purpose; they have been successfully used to deliver TNF, IFN-gamma, and IFN-alpha-2a to tumors [2, 3, 13] owing to their ability to recognize an aminopeptidase-N (CD13) form expressed by tumor vessels [14–16]. However, the sulfur atoms of these peptides may bind to gold, thereby altering or hindering the NGR structure. Thus, an alternative molecular scaffold of NGR is necessary. In this regard, a relevant issue is the potential impact of the scaffold on NGR stability and function. Indeed, consistent experimental evidence suggests that the NGR scaffold crucially affects asparagine (N) deamidation, a spontaneous degradation reaction that leads to the formation of aspartate (D) and isoaspartate (isoD). Remarkably, this reaction, which occurs in an unusually rapid manner in NGR peptides (e.g., the half-life of asparagine in CNGRC is 3–4 h) [17, 18], causes a change in function, as the transition from NGR to isoAsp-Gly-Arg (isoDGR) (but not to DGR) is accompanied by receptor switching from CD13 to integrins

[17–20]. Biochemical studies, NMR structure analyses, and integrin-docking experiments have shown that isoDGR, but not NGR or DGR, can fit into the RGD-binding pocket of αvβ3, an integrin that is overexpressed in tumor vessels, recapitulating not only the canonical RGD/integrin contacts, but also establishing additional polar interactions [21]. Remarkably, isoDGR embedded in different molecular scaffolds have markedly different affinities for αvβ3 and can bind other integrins, such as αvβ5, αvβ6, αvβ8, and α5β1 [17, 18, 21–23]. Even the linker used for peptide coupling to proteins can affect integrin binding [24]. Thus, the molecular scaffold and the linker of NGR might be crucial for peptide/gold interactions, peptide stability, NGR conformation, and CD13 recognition, as well as for the receptor binding properties of the NGR degradation products, with potentially important pharmacological and toxicological implications.

Accordingly, we prepared various TNF/gold-based nanodrugs functionalized with peptides containing NGR (or its degradation product isoDGR) embedded in different scaffolds and characterized their functional properties and their therapeutic activity in experimental models. We show that gold nanoparticles tagged with a novel head-to-tail cyclic NGR peptide can be used as carriers for delivering extremely low doses of TNF to tumors, with evidence of activity. Furthermore, we provide evidence that the mechanism of action is primarily mediated by CD13 targeting, and not by integrin targeting consequent to isoDGR formation.

2 Results

2.1 Preparation and characterization of NGR and IsoDGR peptides

We prepared new hexa- and epta-peptides (head-to-tail cyclized), called N1, N3, N4, and N5, containing NGR and a Cys residue with a free thiol group that enables peptide coupling to proteins or to nanoparticles by using maleimide-containing bifunctional cross-linkers (see Fig. 1 for a schematic representation). In parallel, we prepared two disulfide-bridged peptides (called NGR-2C and NGR-2C(Y)), and two isoDGR peptides corresponding to the main deamidation products of N1 and N3 (called Iso1 and Iso3) (Fig. 1), previously described [17, 18, 24], which can be used
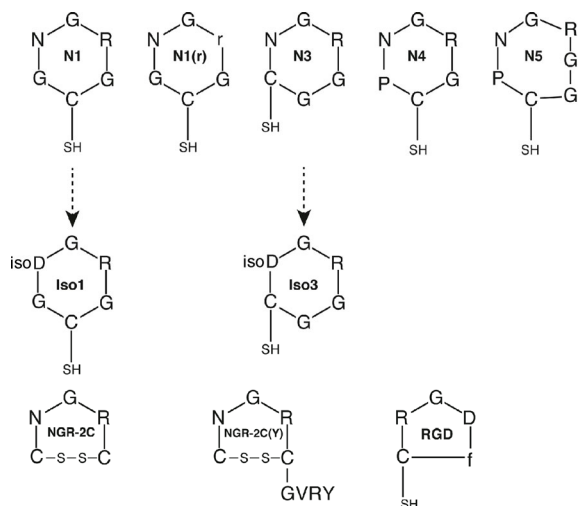
Figure 1 Schematic representation of NGR, isoDGR, and RGD peptides with different molecular scaffolds prepared by chemical synthesis. Amino acids are represented with the single letter code; SH, free thiol group; isoD, isoaspartate; r, D-arginine; f, D-phenylalanine. Peptide codes are reported within each structure. Arrows indicate the isoDGR deamidation products of N1 and N3.

as positive controls in CD13 and integrin binding studies. Other control peptides, including a mutated form of N1 with D-Arg in place of L-Arg (called N1(r)) and a peptide with RGD in place of NGR (CRGDf, called RGD), all cyclic and with a free thiol, were also prepared (Fig. 1). A mass spectrometry analysis of each product showed molecular masses consistent with the expected values (Table S1 in the Electronic Supplementary Material (ESM)).

The capability of NGR peptides to recognize CD13 was analyzed by enzyme inhibition and competitive binding assays. We observed that the peptides N1 and N3 were the most efficient inhibitors and binders (Fig. 2(a) and Table S2 and Fig. S1 in the ESM). Noteworthy, while N3 inhibited CD13 with potency similar to that of NGR-2C(Y), a reference peptide, N1 was about 5–6-fold more efficient, pointing to an important role of the NGR molecular scaffold in CD13 recognition. N4, N5, N1(r), and RGD caused little or no inhibition (Figs. 2(a) and 2(b)). Based on a steady-state enzyme kinetic analysis in the presence of various amounts of substrate and inhibitors, N1, N3, and NGR-2C affected the Michaelis constant (K_m), but not the maximum velocity (V_{max}) (Fig. 2(c)). The data were consistent with the competitive inhibition model (N1, K_i = 12.4 ± 5.4 μM; N3, K_i = 81.3 ± 12.1; NGR-2C, K_i = 134 ± 28), suggesting that N1, N3, and NGR-2C bind

within, or close to, the active site of the enzyme.

To exclude the possibility that the differential binding properties of N1, N3, and NGR-2C(Y) were related to differential Asn deamidation (with consequent NGR-to-DGR/isoDGR transition and loss of affinity), we studied their deamidation kinetics. A mass spectrometry analysis of peptides before and after incubation in ammonium bicarbonate buffer, a condition known to promote rapid peptide deamidation, showed a 1-Da increase in the molecular mass of each NGR site after 22 h of incubation (Fig. S2(a) in the ESM). As the transition of N to D/isoD causes the gain of 1 Da, these data suggest that all of the peptides were completely deamidated after incubation. Accordingly, a competitive binding assay to αvβ3 showed that fifty percent of the NGR-to-isoDGR transition occurred after approximately 2 h of incubation for all peptides (Fig. S2(b) in the ESM), pointing to similar kinetics. Thus, the different affinities of these peptides to CD13 were not related to differential kinetics of Asn deamidation. More likely, they were related to the different scaffolds, which could affect the NGR structure or directly contribute to CD13 binding. The higher affinity of N1 (with G before NGR) compared to N3 and NGR-2C (both with C before NGR) suggests that a G/C change at this position markedly affects binding. In contrast, the similar affinity of N3 and NGR-2C (with G or C after NGR, respectively) suggests that the G/C change at this position is less important.

The capability of N1, N3, Iso1, and Iso3 to recognize integrins was also characterized by an αvβ3-competitive binding assay. Micromolar concentrations of N1 competed with the binding of a CisoDGRC-peroxidase conjugate to αvβ3 (EC$_{50}$: 10 μM) (Fig. S3 in the ESM). The apparent binding was likely indirect and related to the formation of a small amount (0.1%) of isoDGR during the assay, as Iso1 inhibited binding at 1,000-fold lower concentrations (EC$_{50}$: about 10 nM). Similar results were obtained with N3 and Iso3 (Fig. S3 in the ESM).

2.2 Preparation and characterization of NGR- and IsoDGR-albumin conjugates

The peptides N1 and N3 and the corresponding Iso1 and Iso3 deamidation products were selected for gold functionalization. Given the capability of gold
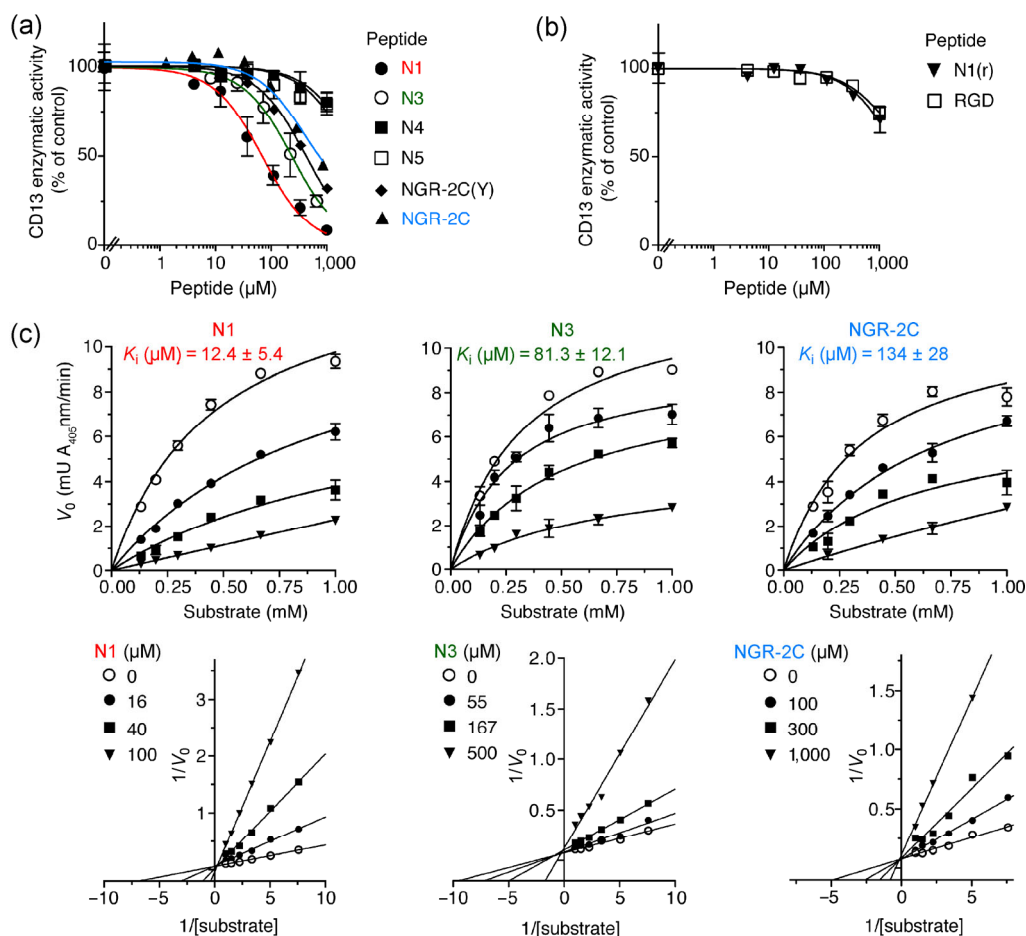
Figure 2 Effect of NGR peptides with different molecular scaffolds on CD13 enzymatic activity. Recombinant human histidine-tagged CD13 (200 ng/mL) was mixed with different amounts of peptides. The mixture were then added to a solution containing the L-alanine p-nitroanilide substrate and incubated for 30 min ((a) and (b)) at 37 °C, or 5 min at room temperature (c). The formation of p-nitroanilide product was quantified spectrophotometrically (A405 nm). (a) and (b) Representative experiments (n = 2–3) are shown (mean ± SE). See also Table S2 in the ESM. (c) Steady state kinetic analysis of CD13 in the presence of various amounts of L-alanine p-nitroanilide substrate and N1, N3, or NGR-2C peptide. Representative plots of initial velocity (V_0) versus substrate concentration ((c), upper panels) and double reciprocal plot ((c), lower panels) (mean ± SE, in quadruplicate). The inhibitory constant (K_i) reported in the plot is the result of two independent experiments (mean ± SE).

nanoparticles to strongly bind human serum albumin (HSA), we prepared peptide-HSA conjugates (called N1-, N3-, Iso1-, and Iso3-HSA) using sulfosuccinimidyl-4-[N-maleimidomethyl]cyclohexane-1-carboxylate (sulfo-SMCC) as a bifunctional cross-linker, and used these conjugates for nanogold functionalization. In parallel, we prepared a sulfo-SMCC-activated HSA lacking the targeting peptide (called *HSA) as a control. Analytical gel-filtration high-performance liquid chromatography and mass spectrometry showed that all peptide-albumin conjugates consisted of monomeric albumin modified with 5–6 linkers and 2–6 peptide molecules (Figs. S4(a) and S4(b) in the

ESM). Integrin binding assays showed no binding of N1- and N3-HSA to αvβ3, even at concentrations of 3,000 nM, whereas Iso1-HSA and Iso3-HSA could bind αvβ3 with K_i values of approximately 5 nM (Table 1). These data suggest that isoDGR contaminants in the NGR conjugates were <0.1%. However, N1- and N3-HSA, after forced deamidation in ammonium bicarbonate buffer (16 h at 37 °C), could bind αvβ3 with K_i values of approximately 5 nM (Table 1), similar to the isoDGR counterparts. Furthermore, when we performed deamidation studies in cell culture medium (Dulbecco's modified Eagle medium, DMEM) at 37 °C, i.e., in physiological conditions, we observed that the

Table 1 Binding of N1-, N3-, Iso1-, and Iso3-HSA to different integrins as measured by a competitive binding assay using a CisoDGRC-HRP conjugate

Competitor	Competitive binding (K_i [a] values in nM) to									
	αvβ3		αvβ5		αvβ6		αvβ8		α5β1	
	n [b]	K_i	n	K_i	n	K_i	n	K_i	n	K_i
N1-HSA	1	>3,000 [c]		nd [d]		nd		nd		nd
N1-HAS (37 °C) [e]	2	3.9 ± 0.9		nd		nd		nd		nd
N3-HSA	1	>3,000		nd		nd		nd		nd
N3-HSA (37 °C)	2	6.1 ± 1.9		nd		nd		nd		nd
Iso1-HSA	6	4.8 ± 0.9 (1) [f]	3	25.5 ± 5.6 (5.3)	4	1,445 ± 666 (301)	2	29,086 ± 1875 (6059)	3	172 ± 29 (36)
Iso3-HSA	3	4.7 ± 1.8 (1)	2	7.1 ± 1.6 (1.5)	3	127 ± 43 (27)	4	116 ± 4 (25)	3	39 ± 5.1 (8.3)
*HSA	1	>10,000	1	>10,000	1	>10,000	1	>10,000	1	>10,000

[a] K_i, equilibrium dissociation constant of the competitor (mean ± SE). K_i was determined using a competitive binding assay as described previously [24]. [b] n, number of independent experiments (each in duplicate). [c] >, maximum concentration tested that had no inhibitory effect. [d] nd, not determined. [e] 37 °C, the conjugate was incubated overnight at 37 °C in 0.1 M ammonium bicarbonate buffer, pH 8.5, to favor NGR-to-isoDGR conversion. [f] Relative values to αvβ3 K_i.

half-lives of N1- and N3-HSA were 10 and 15 h, respectively (Fig. S4(c) in the ESM). These data indicate that no significant deamidation occurred during conjugate preparation and that significant deamidation may occur during lengthy *in vitro* or *in vivo* assays. Thus, the potential transition of NGR to isoDGR during assay incubation was taken into account in all subsequent studies.

To assess the capability of NGR peptide-albumin conjugates to recognize CD13 on cell membranes, we analyzed the interactions of each conjugate (labeled with the fluorescent compound IRDye 680) with human umbilical vein endothelial cells (HUVECs) and human breast adenocarcinoma cells (MCF-7), i.e., with CD13-positive and -negative cells. Based on a preliminary characterization of these cells by a FACS analysis with specific antibodies; HUVECs were CD13+, αvβ3+, αvβ5+, and α5β1+, whereas MCF7 cells were CD13−, αvβ3−, αvβ5+, and α5β1+ (Fig. 3(a)).

Interestingly, cell binding assays with fluorescent conjugates showed that N1-HSA (140 nM) could weakly bind HUVECs (CD13+), but not MCF-7 cells (CD13−) (Fig. 3(b)). In contrast, N3-HSA (140 nM) could bind both cell lines (Fig. 3(b)). The unexpected binding of 140 nM N3-HSA to CD13− cells likely accounted for isoDGR formation during the assay, as suggested by the observation that Iso3-HSA (the deamidation product of N3-HSA) could significantly bind MCF-7 cells, even at sub-nanomolar levels (Fig. 3(c)). Indeed, considering the rapid deamidation kinetics of N3 in cell culture medium (see above), it is very likely that the nonspecific binding of 140 nM N3-HSA to CD13− cells was related to the formation of 1%–2% Iso3-HSA during assay incubation; it is a high-affinity ligand of αvβ5 and α5β1 (see Table 1 for integrin binding affinity), both of which are expressed by MCF-7 cells. In contrast, Iso1-HSA could bind MCF-7 cells only at concentrations of >50 nM (Fig. 3(c)), likely owing to its low affinity for αvβ5 and α5β1 (Table 1) and the lack of αvβ3 on these cells.

These data suggest that N1- and N3-HSA generate degradation products with different integrin receptor affinities and specificities, which may confound the interpretation of NGR interactions with membrane CD13. Thus, to clarify this point, we performed additional binding experiments using human acute lymphoblastic leukemia cells (MOLT-4), a cell line that does not express αvβ3-integrin (not shown), transfected with or without human CD13 cDNA (CD13/MOLT-4). Although a FACS analysis clearly showed the expression of CD13 by the transfected cells (Fig. S5(a) in the ESM), no binding was observed with 140 nM
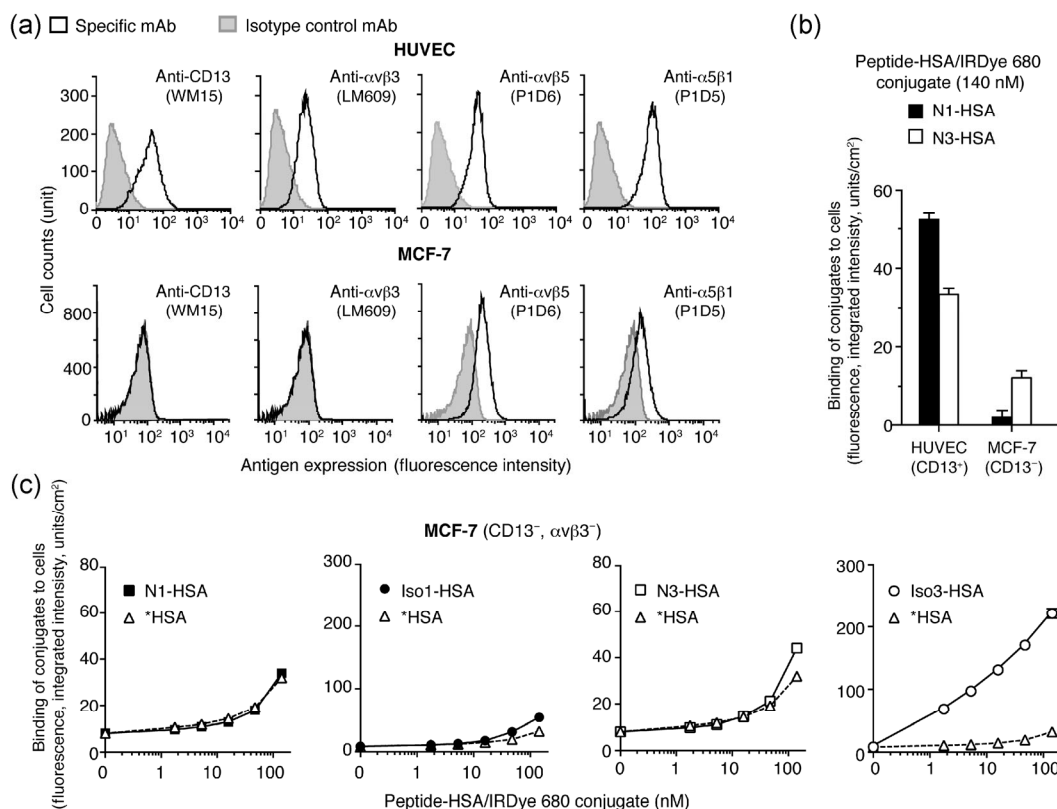
Figure 3 Binding of N1-, Iso1-, N3-, and Iso3-HSA to HUVECs and MCF-7. (a) Expression of CD13, αvβ3, αvβ5, and α5β1 by HUVECs and MCF-7 cells, as evaluated by a FACS analysis using the indicated mouse monoclonal antibody, followed by AlexaFluor 488-goat anti-mouse IgG polyclonal antibody. (b) and (c) Binding of the indicated peptide-HSA/IRDye 680 conjugate to HUVECs and MCF-7 cells. A dose of 140 nM (b) or various amounts (c) of conjugates were added to cell monolayers (grown in 96-well microtiter plates) and incubated for 1 h at 37 °C, 5% CO_2 (see Experimental section). After washing, fluorescence was measured using an Odyssey CLx (LI-COR) scanner. In (b), the specific binding of N1- and N3-HSA was obtained by subtracting the binding of *HSA.

N1- or N3-HSA/IRDye 680 (Fig. S5(b) in the ESM). Higher concentrations could not be tested owing to the high levels of nonspecific binding of albumin to both cell lines. These data clearly show that low (nanomolar) concentrations of NGR cannot bind the CD13 expressed by these cells *in vitro*.

This finding is consistent with the results of previous studies showing that NGR can recognize with high affinity a CD13 form expressed by the endothelium of tumor vessels, and not (or less efficiently) CD13 expressed by other tissues, which is an important pre-requisite for efficient and selective tumor vascular targeting. To verify that low concentrations of N1 can indeed interact with endothelial cells in tumors, we injected 20 µg of N1-HSA/IRDye 680 or *HSA/IRDye 680 to mice bearing WEHI-164 fibrosarcomas (a dose that generates 100–200 nM peak levels) and analyzed

their binding to tumors, spleens, and kidneys by a fluorescence analysis after organ explantation. Both conjugates accumulated in tumors and, to a lesser extent, in the spleen and kidney (Figs. 4(a) and 4(b)).

Significantly higher N1-HSA/IRDye 680 binding than HSA/IRDye 680 binding was observed in tumors, but not in the spleen or kidney, two CD13-rich organs. A FACS analysis of tumor cells after tissue disaggregation showed an increased accumulation on CD31+CD45− cells (endothelial cells), but not on CD31−CD45− (tumor cells) or CD45+ cells (leukocytes) (Fig. 4(c)). Notably, the relative staining of endothelial cells/leukocytes was significantly higher for N1-HSA/IRDye 680 than controls, but not for *HSA/IRDye 680 compared to controls (Fig. 4(d)). These results suggest that low concentrations of N1-HSA can indeed interact with endothelial cells in tumors.
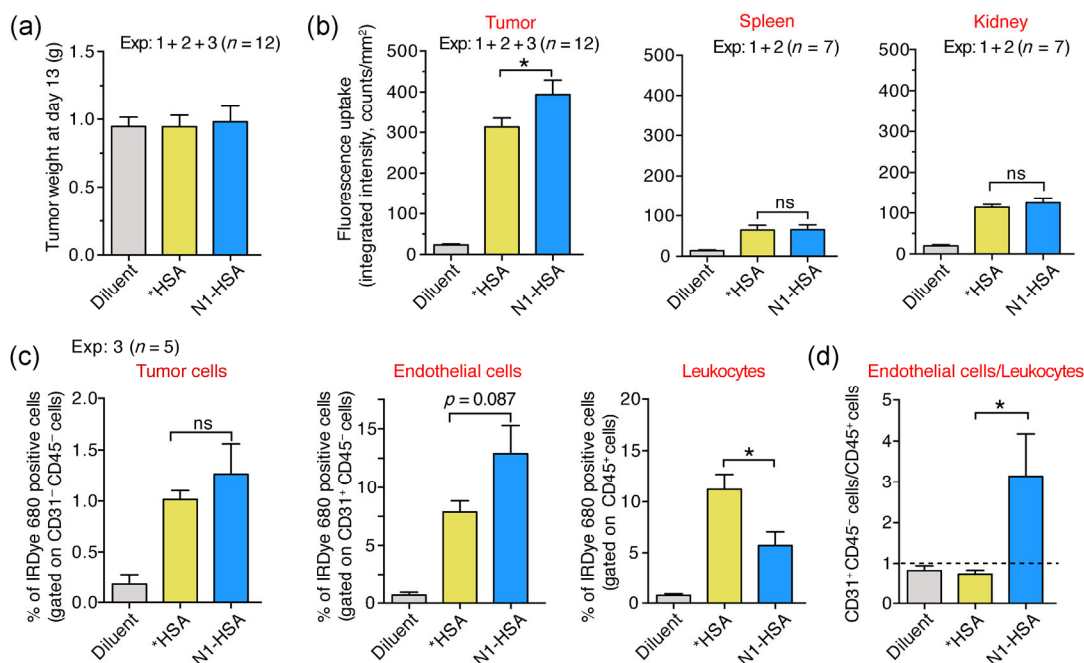
Figure 4 Tumor uptake of N1-HSA/IRDye 680 and *HSA/IRDye 680. (a) and (b) WEHI-164 tumor-bearing mice were injected i.v. with 20 µg of N1-HSA/IRDye 680 or *HSA/IRDye 680 or with diluent. After 24 h, tumors, spleen, and kidneys were explanted, weighted, and analyzed with an Odyssey scanner to quantify the fluorescence uptake. Cumulative result of 2–3 independent experiments as indicated (*n*, number of mice). (c) Tumors were disaggregated and analyzed by FACS using anti-CD31 and anti-CD45 antibodies (see Experimental Section). (d) Ratio between CD31⁺CD45⁻ and CD45⁺ cells (endothelial cells/leukocytes).

2.3 Preparation and characterization of peptide-tagged gold nanoparticles loaded with TNF

Bifunctional gold nanoparticles bearing peptide-HSA and recombinant murine TNF were then prepared for *in vivo* studies. Gold nanoparticles were tagged with peptide-HSA and TNF by incubating colloidal gold with mixtures of these compounds. In particular, four nanodrugs, called N1/, N3/, Iso1/, and Iso3/Au/TNF, were prepared by incubating colloidal gold with TNF solutions pre-mixed with N1-, N3-, Iso1-, or Iso3-HSA, respectively.

The size and the aggregation state of each nanodrug were characterized by UV–visible (UV–Vis) spectrophotometry, dynamic light scattering (DLS), transmission electron microscopy (TEM), and zeta-potential analyses. The UV–Vis absorption spectra for each product showed single peaks at 528–530 nm (Fig. 5(a)) and a 650 nm/530 nm ratio <0.1 (Table 2), which are consistent with products containing small amounts of or no aggregates. Furthermore, TEM showed that gold nanoparticles had an average diameter of approximately 25 nm (Fig. 5(b) and Table 2), and a zeta-potential

analysis showed that all nanodrugs had a similar negative charge (Table 2). These results indicate that the four nanodrugs had very similar physico-chemical properties, and were mono-dispersed. Remarkably, two freezing/thawing cycles and lyophilization/resuspension did not cause nanoparticle aggregation as determined by UV–visible spectrophotometric analysis (not shown).

The presence of functional TNF on gold nanoparticles was checked by a cytotoxicity assay, as well as by anti-TNF antibodies and soluble TNF receptor 2 (sTNF-R2) binding assays. The presence of functional peptides was checked by αvβ3 binding assays (before and after forced deamidation for NGR-containing drugs). The cytotoxicity assay showed that 1–4 and 9–16 bioactive TNF molecules/nanoparticle were present in conjugates prepared at pH 6.0 and pH 6.5 (Table 2). Furthermore, all TNF-bearing nanodrugs could bind TNF receptors (sTNF-R2) spotted onto nitrocellulose filters, suggesting that the receptor-binding properties of TNF were preserved after adsorption on the gold surface (Fig. 5(c), left panel). Of note, after 48 h of incubation of the TNF-bearing nanodrug, 15% of TNF
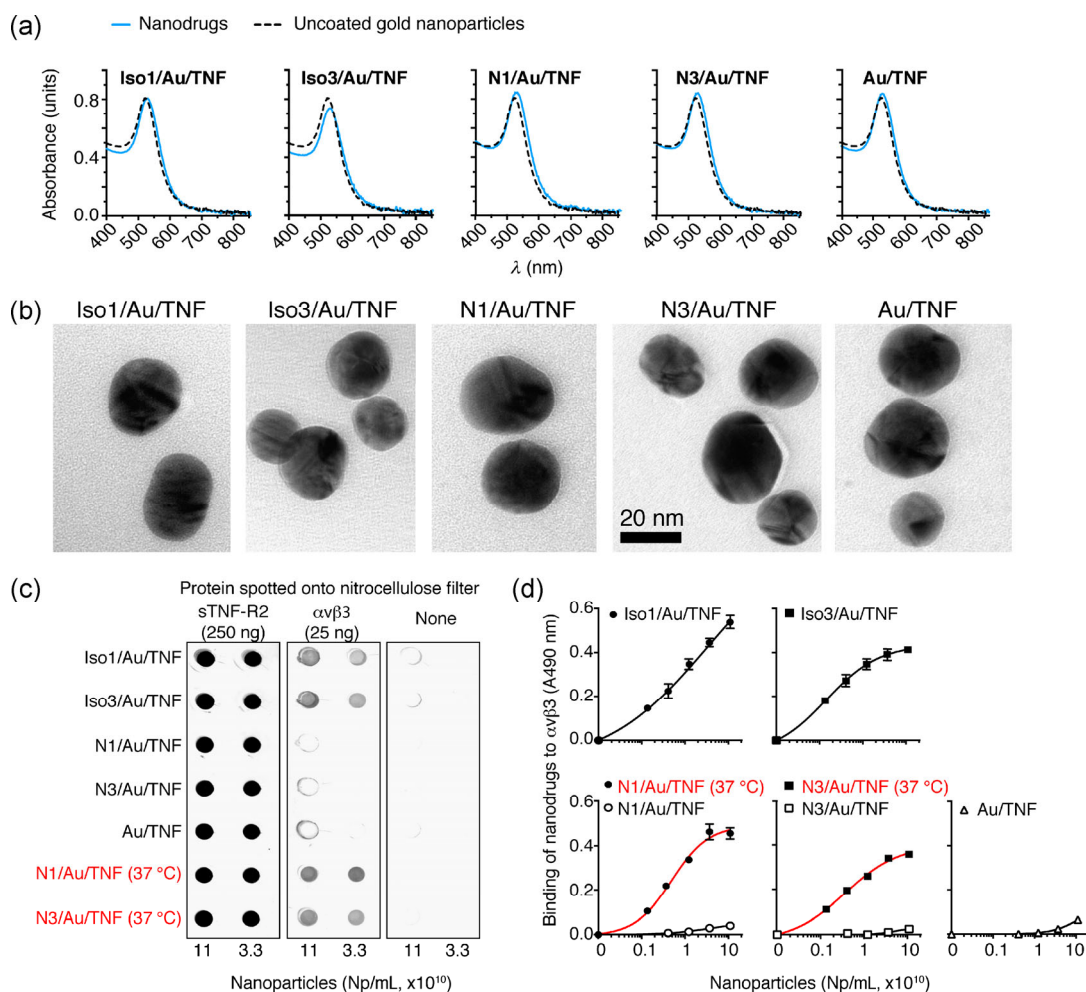
Figure 5 Characterization of TNF-based nanodrugs by UV–Vis spectrophotometry, TEM, and binding assays using αvβ3 and sTNF-R2. (a) UV–Vis absorption spectra of N1/, N3/, Iso1/, Iso3/Au/TNF, and Au/TNF. Dotted line corresponds to uncoated 25-nm gold nanoparticles. (b) A representative microphotograph of each nanodrug. (c) Binding of nanodrugs to sTNF-R2 and αvβ3 spotted onto nitrocellulose filters, as detected by silver staining of gold nanoparticles. The binding of N1/ and N3/Au/TNF after heat-treatment (37 °C), i.e., after forced deamidation, is also shown (in red). (d) Binding of nanodrugs to αvβ3 adsorbed onto microtiter plates as detected with anti-TNF antibodies and HRP-labeled secondary antibodies.

was released in solution (half-life, 10–12 h) (Fig. S6(d) in the ESM). Binding studies to αvβ3 spotted onto nitrocellulose filters showed that Iso1/ and Iso3/Au/ TNF, but not N1/, N3/Au/TNF, and Au/TNF, could bind αvβ3, suggesting that no NGR deamidation occurred during nanodrug preparation (Fig. 5(c), middle panel). However, after forced deamidation, both N1/ and N3/Au/TNF could efficiently bind αvβ3, suggesting that N1- and N3-HSA conjugates were successfully loaded on gold nanoparticles (Fig. 5(c), middle panel). Similar results were also obtained when αvβ3 was adsorbed onto microtiter plates and the binding of each nanodrug was detected using anti-

TNF antibodies (Fig. 5(d)). Taken together, the above results suggest that the bifunctional properties of N1/, N3/, Iso1/, and Iso3/Au/TNF were preserved, i.e., ligand targeting and TNF activity.

2.4 Anti-tumor activity of TNF-based nanodrugs

The *in vivo* antitumor properties of each nanodrug were then investigated using the WEHI-164 fibro-sarcoma model. In the first set of experiments, tumor-bearing mice were treated (i.v.) with a dose of nanodrugs equivalent to 5 pg of bioactive TNF, a dose that is completely inactive in this model when free TNF is used. Interestingly, N1/Au/TNF delayed

Table 2 Characterization of TNF-based nanodrugs by UV–Vis spectroscopy, DLS, cytotoxicity assays, TEM, and zeta-potential analyses

Nanodrugs [a]	UV–Vis [b]			DLS [c] Radius (nm)	TNF molecule/Np [d]	TEM [e] Diameter (nm)	Zeta-potential [f] (mV)
	λ_{max} (nm)	PW 75% (nm)	650 nm /530 nm				
(160 µg:16 µg); pH 6.0							
N1/Au/TNF	531 ± 3	59 ± 1.7	0.08 ± 0.02	16.1	−15.9 ± 7.1	1.2 ± 0.2	25.8 ± 1.2
N3/Au/TNF	531 ± 3	59 ± 0.4	0.09 ± 0.01	17.7	−14.5 ± 6	1.1 ± 0.2	26.2 ± 1.0
Iso1/Au/TNF	528 ± 1	59 ± 0.7	0.09 ± 0.01	21.6 ± 3.9	−15.2 ± 6.7	3.4 ± 0.7	25.4 ± 1.1
Iso3/Au/TNF	530 ± 2	59 ± 0.4	0.06 ± 0.01	16.8	nd	2.8 ± 0.4	nd [g]
Au/TNF	528 ± 2	58 ± 0.1	0.09 ± 0.01	22.1	−13.1 ± 5.2	3.6 ± 0.7	27.5 ± 1.1
(160 µg:32 µg); pH 6.5							
N1/Au/TNF	529 ± 2	57.7	0.09	16.4	−16.7 ± 5.5	9.0 ± 2.9	24.9 ± 1.0
Iso1/Au/TNF	526 ± 1	58 ± 0.7	0.09 ± 0.03	23.1	−15.6 ± 6.2	16.3 ± 1.4	27.2 ± 1.0
Uncoated gold	523 ± 2	57 ± 1.2	0.07 ± 0.02	15.5 ± 1.6	nd	0	nd

[a] Nanodrugs were prepared by mixing peptide-HSA and TNF at the indicated ratios with 1 mL of gold (pH 6.0 or 6.5, as indicated).
[b] λ_{max}, wavelength of peak absorbance; PW 75%, peak-width at 75% of height; mean ± SD. [c] Mean ± SD of 2 independent analyses.
[d] Number of bioactive TNF molecules/nanoparticle, as determined by a cytotoxicity assay [25], mean ± SE (5–8 independent experiments).
[e] Particle diameter was obtained by measuring the width of about 30 particles using ImageJ software. Mean ± SE. [f] Mean ± SD. [g] nd, not determined.

tumor growth more efficiently than N3/Au/TNF and Au/TNF (Fig. 6(a)). The stronger activity of N1/ versus N3/Au/TNF is consistent with the CD13 binding properties of the peptides observed *in vitro*, and N1 was 3–4-fold more efficient than N3 with respect to CD13 recognition (Table S2 in the ESM). Furthermore, the stronger activity of N1/Au/TNF compared to Au/TNF suggests that the peptide-mediated "active" targeting mechanism is important for its anti-tumor activity. We also observed that 5 pg of Iso1/Au/TNF, i.e., the main degradation product of N1/Au/TNF, delayed tumor growth to a similar extent or even stronger than N1/Au/TNF (Fig. 6(a)), suggesting that this degradation product is biologically active. Notably, Iso3/Au/TNF was less active then Iso1/Au/TNF.

Based on dose-escalation studies using nanodrugs loaded with 1–4 or with 9–16 TNF molecules/ nanoparticle, the dose-response curves for each drug tended to be U-shaped (Fig. 6(b)). Similarly, NGR-TNF (CNGRCG-TNF fusion protein) showed a U-shaped dose-response curve (Fig. 6(b)). We have previously demonstrated that the U-shaped dose-response curve of NGR-TNF is related to the activation of counter-regulatory mechanisms by high doses, such as soluble receptor shedding, which inhibits TNF activity [1]. The same likely applies to TNF-based nanodrugs. Interestingly, nanodrugs with a fewer TNF molecules/ nanoparticle were more efficient (Fig. 6(b)), likely because a higher number of injected nanoparticles was necessary to achieve the same TNF dose and, consequently, to increase the active/passive targeting effect. No evidence of toxicity, as judged by animal weight loss, was observed for any tested dose and drug. Remarkably, 1 pg of Iso1/Au/TNF induced anti-tumor effects similar to that of 10–20 pg of N1/Au/TNF (Fig. 6(b)), suggesting that Iso1 is more efficient than N1 with respect to ligand targeting. This observation raises the question as to whether N1/Au/TNF activity was actually mediated by the *in vivo* formation of Iso1/Au/TNF and integrin targeting, rather than N1/ CD13 interactions. To rule out this possibility, we performed CD13 neutralization experiments with a) the antibody R363, an anti-murine CD13 antibody previously used to neutralize the anti-tumor activity of NGR-TNF and NGR-IFNgamma [2, 3], and b) with an excess of free N1 peptide. The anti-tumor activity of N1/Au/TNF was inhibited by co-administration with either the R363 or N1 peptide (Figs. 6(c) and 6(d)),
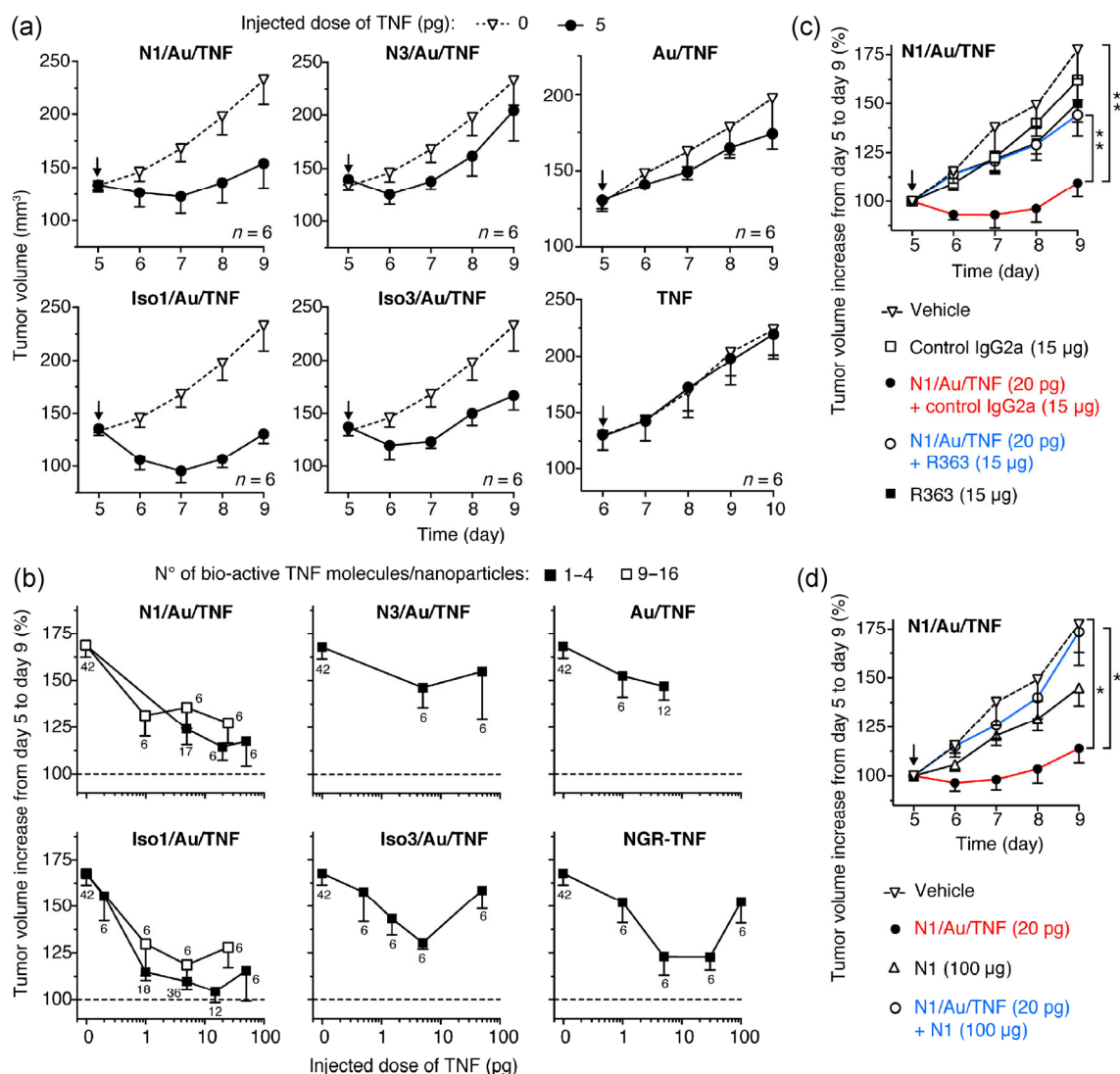
Figure 6 Anti-tumor effects of various formulations of TNF (N1/, N3/, Iso1/, Iso3/Au/TNF nanodrugs, TNF, and NGR-TNF) alone ((a) and (b)) or in combination with the neutralizing anti-CD13 antibody R363 (c) or peptide N1 (d) in the WEHI-164 fibrosarcoma model. (a) Anti-tumor effects of intravenous administration of the indicated drugs, at a dose corresponding to 5 pg of bioactive TNF. Arrows, time of treatment; tumor volumes (mean ± SE, 6 mice/group). (b) Effect of various doses of the indicated nanodrugs (bearing 1–4 or 9–16 bioactive TNF molecules/nanoparticle) on the growth of tumors from day 5 to day 9. Dotted line: normalized tumor volumes at day 5. Numbers within the panels indicate the number of mice per dose (cumulative results of 1–7 independent experiments, with 6 mice/experiment, mean ± SE). (c) and (d) WEHI-tumor-bearing mice were treated at day 5 with N1/Au/TNF alone, in combination with mAb R363 (anti-murine CD13), with isotype matched control antibody (IgG2a), or with N1 at the doses indicated in each panel. Antibodies were given 2.5 h before N1/Au/TNF, whereas N1 was co-administered with N1/Au/TNF. Arrows indicate the day of treatment. Tumor volumes (mean ± SE). The area under the curve for each mouse was calculated using GraphPad Prism. Differences between calculated areas were evaluated by Mann–Whitney tests (6–8 animals per group; **, $P < 0.01$; *, $P < 0.05$).

suggesting that the main mechanism underlying the activity of this nanodrug is indeed related to CD13 targeting, as originally hypothesized. Finally, to assess whether tumor cell targeting was necessary to induce anti-tumor effects, we performed an *in vivo* experiment using the RMA lymphoma model, taking advantage

of the lack of CD13 and αv-integrin expression in RMA cells [2, 19]. We observed that 5 pg of N1/Au/TNF, but not Au/TNF, could induce anti-tumor effects, suggesting that endothelial cell targeting is likely sufficient to induce anti-tumor effects (Fig. S7 in the ESM).

3 Discussion

To tag TNF-bearing gold nanoparticles with a CD13 ligand, we selected the head-to-tail cyclized exa-peptide c(CGNGRG), called N1, which contains a free thiol group suitable for nanodrug coupling. The results of enzyme binding and inhibition experiments performed with recombinant soluble CD13 suggest that this peptide binds within, or close to, the active site (K_i = 12.4 µM) 6–10-fold more efficiently than CNGRC (NGR-2C), a reference disulfide-bridged peptide, and c(CNGRGG) (N3), a similar head-to-tail cyclized exa-peptide. Additionally, *in vivo* studies performed in tumor-bearing mice showed that gold nanoparticles coated with N1-HSA, a peptide-albumin conjugate, can deliver TNF to tumors more efficiently than nanoparticles coated with N3-HSA or with HSA alone. Interestingly, the observation that N1-tagged nanoparticles can deliver extremely low, yet pharmacologically active doses of TNF to tumors (e.g., 5 pg) implies that high-affinity interactions occurred between the N1/Au/TNF nanodrug and tumors. Furthermore, the finding that this effect was inhibited by the co-administration of an excess of N1 points to an important role of the N1 ligand in nanodrug delivery to tumors. This view is also supported by the observation that N1-HSA/IRDye 680, but not HSA/IRDye 680, could bind to the expected targets, i.e., CD31$^+$CD45$^-$ cells in tumors (endothelial cells).

The high-affinity interactions of these conjugates with tumor tissues cannot be explained by the NGR/CD13 interactions observed in the *in vitro* experiments, which showed binding at micromolar concentrations and very weak (or undetectable) interactions at nanomolar levels. One explanation is that NGR binding affinity differs between the CD13 expressed *in vivo* by tumor vessels and the soluble recombinant CD13 or the CD13 form expressed by cells in our *in vitro* studies. This hypothesis is supported by the results of previous studies showing that phage viral particles displaying the NGR peptide can bind CD13-positive endothelial cells isolated from tumors, but not CD13-positive myeloid-derived cells [26]. Other previous studies on the NGR bio-distribution have also shown that this peptide sequence can efficiently bind CD13

in tumors, but not (or less efficiently) other CD13-positive tissues [15]. The structural determinants of the differential binding are unknown. An interesting possibility is that conformational changes in different tissues, possibly owing to tissue-specific cofactors or signaling molecules, results in differential NGR binding affinity. Indeed, natural CD13 is a type II membrane dimeric glycoprotein with an N-terminal membrane anchor, resulting in an arch-like structure on the cell surface that may undergo large conformational changes because each monomer can assume open or closed conformations [27].

Other receptors expressed by endothelial cells might also contribute to the high-avidity interactions of N1/Au/TNF with tumor endothelial cells; for example, considering that this nanodrug contains albumin and TNF, albumin receptors (such as albondin, gp30, and gp18) [28] and membrane TNF receptors (TNF-R1 and TNF-R2) could be involved. In any case, the observation that N1/Au/TNF is more potent than Au/TNF in tumor animal models, and that the anti-CD13 antibody R363 or an excess of free N1 peptide completely reduces its activity to the level of Au/TNF points to a major contribution of NGR/CD13 interactions in tumor drug delivery.

Although N1 characterization studies showed no binding to integrins at submicromolar concentrations, the notion that N1 can deamidate to generate Iso1, a high-affinity integrin ligand, and the observation that Iso1/Au/TNF acts as a potent nanodrug active at picogram doses in our animal models raises the question as to whether integrin binding contributes to N1-mediated targeted delivery. The marked inhibition of N1/Au/TNF by the anti-CD13 antibody R363 and by N1 suggests that the main mechanism underlying the activity of this nanodrug is related to CD13 targeting, as originally hypothesized, and not (or minimally) to integrin targeting. In previous studies, we have shown that the anti-tumor activity of a CNGRC-TNF fusion protein can be inhibited by an excess of CNGRC, but not of CisoDGRC (integrin ligand), whereas the activity of CisoDGRC-TNF can be inhibited by an excess of CisoDGRC, but not of CNGRC [19]. These results suggest that the binding of NGR to CD13 alone is sufficient for targeting and

that the transition to isoDGR and consequent integrin recognition is not necessary for the observed activity.

Another important point is related to the impact of the number of TNF molecules/nanoparticles on nanodrug activity. Indeed, injecting the same dose of TNF formulated as a nanodrug bearing 1–4 or 9–16 TNF molecules/nanoparticle implies that a different number of nanoparticles are injected (e.g., 2–3 × 10⁶ or 2–3 × 10⁷ nanoparticles, respectively, for a dose of 5 ng of TNF). This may have important consequences on activity, despite equal TNF doses, for the following reasons: (1) A higher number of injected nanoparticles could reach a higher number of endothelial cells in tumors and (2) a lower number of TNF molecules/ nanoparticles allows the loading of a higher number of peptide-albumin molecules on each nanoparticle, thereby increasing the overall targeting efficiency. Consistent with this view, we observed stronger effects with the nanodrug bearing 1–4 TNF molecules/ nanoparticle.

In conclusion, the results show that the N1 peptide has an improved affinity for CD13, is suitable for tagging colloidal gold, and (after coupling to nanogold) is an efficient carrier for TNF delivery to tumors. The favorable CD13-binding properties of N1 may overcome some of the problems related to the use of CNGRC as a gold-tagging peptide. Indeed, in the case of CNGRC, disulfide-gold interactions and disulfide exchange between adjacent peptides may occur in multivalent nanoparticles, thereby altering or hindering the NGR structure [29, 30]. N1 overcomes this problem because cyclization is obtained via head-to-tail peptide bonds and not via cystine. Finally, the development of N1/ Au/TNF overcomes a major obstacle in the use of TNF in patients, i.e., its low therapeutic index. Indeed, the clinical use of TNF is currently limited to loco-regional treatments in patients with sarcomas localized at the extremities owing to the prohibitive systemic toxicity. As no toxic reactions were observed in mice treated intravenously with extremely low doses of N1/Au/ TNF, this drug formulation could enable, in principle, systemic treatments of cancer patients with solid tumors. N1-tagged nanogold could potentially be loaded with other synergistic cytokines (e.g., IFN-gamma or EMAP-2), thereby enabling multicytokine delivery to endothelial cells in tumors.

4　Experimental

4.1　Cell lines and reagents

MCF-7 and murine WEHI-164 fibrosarcoma cells were cultured in DMEM supplemented with 10% fetal bovine serum, 2 mM glutamine, 50 µg/mL streptomycin, 100 U/mL penicillin, and 0.25 µg/mL amphotericin-B. HUVECs were cultured in endothelial cell growth medium (EGM)-2 (Lonza, Walkersville, MD, USA). MOLT-4 cells (acute lymphoblastic leukemia) trans-fected with human CD13 cDNA (CD13/MOLT-4) were prepared and cultured as described previously [15].

Sulfo-SMCC was obtained from Pierce (Rockford, IL, USA), HSA was obtained from Baxter (Deerfield, IL, USA), and bovine serum albumin (BSA) was obtained from Sigma (St. Louis, MO, USA).

Murine tumor necrosis factor-alpha (TNFα) was prepared as described previously [25]. TNF was dialyzed against 5 mM citrate buffer, pH 6.0 and stored in aliquots at –20 °C.

NGR-TNF (consisting of TNF fused with the C-terminus of CNGRCG) was prepared by recombinant DNA technology and purified from *Escherichia coli* cell extracts as described previously [2].

Human αvβ3, αvβ5, and α5β1 integrins were obtained from Immunological Sciences (Rome, Italy); recombinant human αvβ6 and αvβ8 integrins were obtained from R&D Systems (Minneapolis, MN, USA). Monoclonal antibodies WM15 and R363 (anti-human and -mouse CD13, respectively) were obtained from Acris Antibodies (San Diego, CA, USA), LM609, P1D6, and P1D5 (anti-human αvβ3, αvβ5, and α5β1, respectively) were obtained from Immunological Sciences (Rome, Italy), and rat IgG2a isotype control antibody was obtained from BioLegend (San Diego, CA, USA).

4.2　Peptide synthesis and characterization

Head-to-tail cyclic peptides (see Fig. 1 for schematic representations of each peptide and peptide code) were prepared by the solid-phase Fmoc method [31]. Disulfide-bridged NGR peptide was prepared as described previously [18]. All peptides were dissolved in water and stored in aliquots at –20 °C. The molecular mass of each peptide was checked by MALDI-TOF

mass spectrometry (see Table S1 in the ESM). Thiol-containing peptides were quantified using the Ellman's assay.

4.3 CD13 enzymatic activity assay and CD13 competitive binding assay

For the CD13 enzymatic activity assay, 96-well PVC microtiter plates were filled with a mixture of recombinant human His-tagged CD13 (0.2 µg/mL, Sino Biological Inc., Beijing, China), L-alanine-p-nitroanilide (0.5 mM; Sigma) and various amounts of peptide in 60 mM potassium phosphate buffer, pH 7.4 (100 µL/well, final volume). The mixtures were then incubated for 30 min at 37 °C. The absorbance at 405 nm of the p-nitroanilide product was measured using an enzyme-linked immunosorbent assay microtiter plate reader. The IC_{50} was calculated by a non-linear regression analysis of competitive inhibition data using GraphPad Prism (GraphPad Software, Version 6.00; San Diego, CA, USA).

Steady-state enzyme kinetic analyses were performed at room temperature (23 °C) in 96-well plates as described above, using increasing concentrations of L-alanine-p-nitroanilide (100–1,000 µM), at fixed concentrations of N1 ranging from 0 to 100 µM. The initial velocities (V_0) were calculated from the slopes of the first 5 min of the reaction. The enzyme inhibitory constants (K_i) were calculated using the Competitive enzyme inhibition model of GraphPad Prism (GraphPad Software, Version 6.00).

A CD13 competitive binding assay with peptides was performed using microtiter plates coated with the anti-CD13 monoclonal antibody WM15 and His-tagged recombinant CD13 as described in the ESM.

4.4 Preparation of peptide-HSA conjugates and characterization of their CD13 and integrin binding properties

Peptide N1, N3-, Iso1-, and Iso3- were coupled to HSA as follows: HSA, 40 mg in 380 µL of 10 mM phosphate buffer, 138 mM sodium chloride, 2.7 mM potassium chloride, pH 7.4, containing 5 mM EDTA (PBS-E) was mixed with sulfo-SMCC (2.4 mg in 120 µL in water) and left to react for 1 h at room temperature.

Then, the mixture was purified by gel-filtration chromatography on a NAP-5 column (GE Healthcare Life Sciences, Little Chalfont, UK), pre-equilibrated with PBS-E. Aliquots of activated-HSA (20 mg) were mixed with various peptides (1.5 mg, 9:1 peptide/HSA molar ratio) and reacted for 3 h. Then, 2-mercaptoethanol was added (1 mM, final concentration) and incubated for 0.5 h. The conjugates were gel-filtered through a PD10 column (GE Healthcare Life Sciences) pre-equilibrated with 10 mM phosphate buffer, 138 mM sodium chloride, 2.7 mM potassium chloride, pH 7.4, and stored at −20 °C. The protein concentration in each conjugate was determined spectrophotometrically (A280 nm).

The binding of peptide-HSA to cells was performed as follows: First peptide-HSA conjugates were labeled with the IRDye 680 RD-NHS-ester dye (LI-COR, Lincoln, NE, USA) by incubating mixtures of 590 µL of each conjugate (1.350 mg in of 25 mM Hepes, containing 150 mM NaCl, pH 7.4 (Hepes buffer) with 90 µL of dye (2 mg/mL in dimethyl sulfoxide, 9:1 dye to HSA molar ratio) for 4 h at 4 °C, and blocking with 1 M glycine (50 mM, final concentration, for 0.5 h). The conjugates were then dialyzed extensively against Hepes buffer (10 kDa, cut-off) and stored at −80 °C.

The binding of peptide-HSA/IRDye 680 conjugates to HT-1080, HUVECs, and MCF-7 cells was then analyzed as follows. The cells were grown in 96-well clear-bottom black plates (2–3 × 10^4 cells/well, plated 48 h before the experiment). After washing with DMEM containing 1% fetal bovine serum and 3 mg/mL HSA (binding buffer), each conjugate (0.2–150 nM in binding buffer) was added to the cells, followed by incubation for 1 h at 37 °C, 5% CO_2. After three washings with binding buffer (3 min each), the cells were fixed with PBS containing 2% paraformaldehyde and 3% sucrose for 15 min at room temperature. Binding of conjugates to cells was quantified by scanning the plate with an Odyssey CLx (LI-COR). Then, the cells were counterstained with 4′,6-diamidino-2-phenylindole (DAPI, a nuclear stain) and the plates were analyzed using a VICTOR3 (Perkin Elmer, Waltham, MA, USA) fluorescence plate reader to quantify the cell number in each well.

4.5 Quantification of N1-HSA/IRDye 680 conjugate uptake in tumors and tumor cell suspensions

WEHI-164 tumor-bearing mice were treated i.v. with 20 μg of N1-HSA/IRDye 680 or *HSA/IRDye 680 or with diluent. After 24 h, the tumor, spleen and kidney were collected and analyzed with an Odyssey CLx scanner to assess the uptake of fluorescence (settings: 2 mm; 1.5 intensity; 700-nm filter). Then, tumors were minced, resuspended with a collagenase-D solution in RPMI medium (1 mg/mL, 3 mL/g tumor tissue, Roche, Basel, Switzerland) and incubated for 1 h at 37 °C under gentle agitation. Cell suspensions were filtered through a 70-μm nylon cell-strainer and centrifuged. The pellets were resuspended in PBS containing 2% FCS, Fc-blocking solution (5 μg/mL, BD Biosciences, Franklin Lakes, NJ, USA) and incubated for 10 min at room temperature. After washing, the cells were incubated with the fluorescence labeled-monoclonal antibodies anti-CD45-V500 (2 μg/mL, clone, 30-F11, BD Biosciences) and anti-CD31-FITC (2.5 μg/mL, clone, MEC 13.3; BioLegend, San Diego, CA, USA), both in PBS containing 2% FCS (15 min at room temperature). After washing, the cells were incubated with the dye 7AAD (2.5 μg/mL, BD Biosciences), a marker of dead cells, and analyzed by FACS. At least 100,000 cells/sample were acquired with a FACS Fortessa system equipped FACSDiva software (BD Biosciences). Fluorescence minus-one (FMO) controls were used to gate marker-positive cells. Percentages of stained cells were determined using FlowJo software.

4.6 Preparation of gold nanoparticles functionalized with NGR or isoDGR peptides and TNF

Bifunctional gold nanoparticles bearing peptide-HSA and recombinant murine TNF were prepared by incubating colloidal gold (25 nm; Aurion, The Netherlands) with a TNF solution pre-mixed with N1-, N3-, Iso1-, or Iso3-HSA with the pH of colloidal gold adjusted to 6.0 or 6.5 with 200 mM sodium citrate buffer (100/1 volume ratio). In particular, two protein combination ratios were added to 1 mL of colloidal gold: a) 160 μg of peptide-HSA and 16 μg of TNF with gold pH adjusted to 6.0 and b) 160 μg of peptide-HSA and 32 μg of TNF with gold pH adjusted to 6.5. These ratios were chosen based on the results of preliminary studies performed to identify the concentrations that generate nanodrugs with optimal bifunctional properties and stability (Fig. S6 in the ESM). Mixtures were incubated for 1 h at room temperature under shaking. Then, 100 μL of mPEG-SH solution (15 μg/mL in water, M_W = 20,000, NANOCS) was added to the mixture and incubated for 15 min at room temperature. Finally, 28 μL of a 10% HAS solution was added to saturate the gold nanoparticles. The mixtures were centrifuged twice (12,000 × g for 10 min). The final products were resuspended with 5 mM sodium citrate buffer, pH 6.0, containing 1% HSA to a final volume of 1 mL and stored at −80 °C. Nanoparticles bearing *HSA (lacking the targeting peptide) and TNF were also prepared (Au/TNF).

4.7 Characterization of the physicochemical properties of nanodrugs

The physicochemical properties of each nanodrug were characterized by UV–Vis spectrophotometry, DSL, TEM, and zeta-potential analyses as described in the ESM.

4.8 Characterization of the functional properties of nanodrugs

The number of bioactive TNF molecules loaded onto the nanoparticles was determined by a murine fibroblast LM cytotoxicity assay [25].

The binding of nanodrugs, before and after incubation at 37 °C in 0.1 M ammonium bicarbonate buffer, pH 8.5, to sTNF-R2 and αvβ3 spotted on nitrocellulose filters was performed as described previously [24].

The binding of nanodrugs to microtiter plates coated with αvβ3 as was performed as follows. Human αvβ3 integrin solution and 0.5 μg/mL in PBS with Ca²⁺ and Mg²⁺ (DPBS; Cambrex, East Rutherford, NJ, USA) were added to 96-well microtiter plates (Falcon 3912, Becton Dickinson, 50 μL/well) and incubated overnight at 4 °C. All subsequent steps were carried out at room temperature. The plates were washed with DPBS and further incubated with DPBS containing 3% BSA (200 μL/well; 1 h). The plates were washed with 25 mM Tris-HCl, 150 mM sodium chloride, 1 mM magnesium chloride, 1 mM manganese chloride (pH

7.4; washing solution), and filled with serial dilutions of the nanodrug solution (50 µL/well in washing solution containing 1% BSA, binding buffer). After incubation for 2 h, the plates were washed again and incubated with a rabbit polyclonal anti-TNF serum (IP301) diluted in binding buffer (1:1,000, 50 µL/well, 1.5 h) followed by a goat anti-rabbit peroxidase conjugate diluted in the same buffer (1:1,000, 50 µL/well, 1 h). Bound peroxidase was detected by adding *o*-phenylenediamine chromogenic substrate (70 µL/well).

4.9 Characterization of the pharmacological and toxicological properties of nanodrugs

Studies in animal models were approved by the Ethical Committee of the San Raffaele Scientific Institute, and performed according to the prescribed guidelines. BALB/c female mice (6–7 weeks old; Charles River Laboratories, Calco, Italy) were challenged with subcutaneous injections in the left flank of 1.5×10^6 WEHI-164 cells. Mice were injected, i.v., with nanodrugs diluted with 0.9% sodium chloride containing 100 µg/mL HSA. Tumor growth was monitored by measuring tumor size with calipers. The tumor volume was estimated by calculating $r1 \times r2 \times r3 \times 4/3\pi$, where $r1$ and $r2$ are the longitudinal and lateral radii, and $r3$ is the thickness of the tumor protruding from the surface of normal skin. Animals were sacrificed before tumors reached a diameter of 1.0 to 1.5 cm. Tumor sizes are shown as means ± SE.

Acknowledgements

Electronic Supplementary Material: Supplementary material (regarding additional experimental methods and results) is available in the online version of this article at http://dx.doi.org/10.1007/s12274-016-1035-8.

References

[1] Curnis, F.; Sacchi, A.; Corti, A. Improving chemotherapeutic drug penetration in tumors by vascular targeting and barrier alteration. *J. Clin. Invest.* **2002**, *110*, 475–482.

[2] Curnis, F.; Sacchi, A.; Borgna, L.; Magni, F.; Gasparri, A.; Corti, A. Enhancement of tumor necrosis factor α antitumor immunotherapeutic properties by targeted delivery to aminopeptidase N (CD13). *Nat. Biotechnol.* **2000**, *18*, 1185–1190.

[3] Curnis, F.; Gasparri, A.; Sacchi, A.; Cattaneo, A.; Magni, F.; Corti, A. Targeted delivery of IFNγ to tumor vessels uncouples antitumor from counterregulatory mechanisms. *Cancer Res.* **2005**, *65*, 2906–2913.

[4] Curnis, F.; Gasparri, A.; Sacchi, A.; Longhi, R.; Corti, A. Coupling tumor necrosis factor-α with αV integrin ligands improves its antineoplastic activity. *Cancer Res.* **2004**, *64*, 565–571.

[5] Gregorc, V.; Zucali, P. A.; Santoro, A.; Ceresoli, G. L.; Citterio, G.; De Pas, T. M.; Zilembo, N.; De Vincenzo, F.; Simonelli, M.; Rossoni, G. et al. Phase II study of asparagine-glycine-arginine-human tumor necrosis factor α, a selective vascular targeting agent, in previously treated patients with malignant pleural mesothelioma. *J. Clin. Oncol.* **2010**, *28*, 2604–2611.

[6] Gregorc, V.; Citterio, G.; Vitali, G.; Spreafico, A.; Scifo, P.; Borri, A.; Donadoni, G.; Rossoni, G.; Corti, A.; Caligaris-Cappio, F. et al. Defining the optimal biological dose of NGR-hTNF, a selective vascular targeting agent, in advanced solid tumours. *Eur. J. Cancer* **2010**, *46*, 198–206.

[7] Corti, A.; Curnis, F.; Rossoni, G.; Marcucci, F.; Gregorc, V. Peptide-mediated targeting of cytokines to tumor vasculature: The NGR-hTNF example. *BioDrugs* **2013**, *27*, 591–603.

[8] Giljohann, D. A.; Seferos, D. S.; Daniel, W. L.; Massich, M. D.; Patel, P. C.; Mirkin, C. A. Gold nanoparticles for biology and medicine. *Angew. Chem., Int. Ed.* **2010**, *49*, 3280–3294.

[9] Cai, W. B.; Gao, T.; Hong, H.; Sun, J. T. Applications of gold nanoparticles in cancer nanotechnology. *Nanotechnol. Sci. Appl.* **2008**, *1*, 17–32.

[10] Paciotti, G. F.; Myer, L.; Weinreich, D.; Goia, D.; Pavel, N.; McLaughlin, R. E.; Tamarkin, L. Colloidal gold: A novel nanoparticle vector for tumor directed drug delivery. *Drug Deliv.* **2004**, *11*, 169–183.

[11] Libutti, S. K.; Paciotti, G. F.; Byrnes, A. A.; Alexander, H. R., Jr.; Gannon, W. E.; Walker, M.; Seidel, G. D.; Yuldasheva, N.; Tamarkin, L. Phase I and pharmacokinetic studies of CYT-6091, a novel PEGylated colloidal gold-rhTNF nano-medicine. *Clin. Cancer Res.* **2010**, *16*, 6139–6149.

[12] Powell, A. C.; Paciotti, G. F.; Libutti, S. K. Colloidal gold: A novel nanoparticle for targeted cancer therapeutics. *Methods Mol. Biol.* **2010**, *624*, 375–384.

[13] Meng, J.; Yan, Z.; Wu, J.; Li, L.; Xue, X.; Li, M.; Li, W.; Hao, Q.; Wan, Y.; Qin, X. et al. High-yield expression, purification and characterization of tumor-targeted IFN-α2a. *Cytotherapy* **2007**, *9*, 60–68.

[14] Pasqualini, R.; Koivunen, E.; Kain, R.; Lahdenranta, J.; Sakamoto, M.; Stryhn, A.; Ashmun, R. A.; Shapiro, L. H.; Arap, W.; Ruoslahti, E. Aminopeptidase N is a receptor for tumor-homing peptides and a target for inhibiting angiogenesis. *Cancer Res.* **2000**, *60*, 722–727.

[15] Curnis, F.; Arrigoni, G.; Sacchi, A.; Fischetti, L.; Arap, W.; Pasqualini, R.; Corti, A. Differential binding of drugs containing the NGR motif to CD13 isoforms in tumor vessels, epithelia, and myeloid cells. *Cancer Res.* **2002**, *62*, 867–874.

[16] Di Matteo, P.; Arrigoni, G. L.; Alberici, L.; Corti, A.; Gallo-Stampino, C.; Traversari, C.; Doglioni, C.; Rizzardi, G. P. Enhanced expression of CD13 in vessels of inflammatory and neoplastic tissues. *J. Histochem. Cytochem.* **2011**, *59*, 47–59.

[17] Curnis, F.; Longhi, R.; Crippa, L.; Cattaneo, A.; Dondossola, E.; Bachi, A.; Corti, A. Spontaneous formation of L-isoaspartate and gain of function in fibronectin. *J. Biol. Chem.* **2006**, *281*, 36466–36476.

[18] Curnis, F.; Cattaneo, A.; Longhi, R.; Sacchi, A.; Gasparri, A. M.; Pastorino, F.; Di Matteo, P.; Traversari, C.; Bachi, A.; Ponzoni, M. et al. Critical role of flanking residues in NGR-to-isoDGR transition and CD13/integrin receptor switching. *J. Biol. Chem.* **2010**, *285*, 9114–9123.

[19] Curnis, F.; Sacchi, A.; Gasparri, A.; Longhi, R.; Bachi, A.; Doglioni, C.; Bordignon, C.; Traversari, C.; Rizzardi, G. P.; Corti, A. Isoaspartate-glycine-arginine: A new tumor vasculature-targeting motif. *Cancer Res.* **2008**, *68*, 7073–7082.

[20] Corti, A.; Curnis, F. Isoaspartate-dependent molecular switches for integrin-ligand recognition. *J. Cell Sci.* **2011**, *124*, 515–522.

[21] Spitaleri, A.; Mari, S.; Curnis, F.; Traversari, C.; Longhi, R.; Bordignon, C.; Corti, A.; Rizzardi, G. P.; Musco, G. Structural basis for the interaction of isoDGR with the RGD-binding site of αvβ3 integrin. *J. Biol. Chem.* **2008**, *283*, 19757–19768.

[22] Frank, A. O.; Otto, E.; Mas-Moruno, C.; Schiller, H. B.; Marinelli, L.; Cosconati, S.; Bochen, A.; Vossmeyer, D.; Zahn, G.; Stragies, R. et al. Conformational control of integrin-subtype selectivity in isoDGR peptide motifs: A biological switch. *Angew. Chem., Int. Ed.* **2010**, *49*, 9278–9281.

[23] Bochen, A.; Marelli, U. K.; Otto, E.; Pallarola, D.; Mas-Moruno, C.; Di Leva, F. S.; Boehm, H.; Spatz, J. P.; Novellino, E.; Kessler, H. et al. Biselectivity of isoDGR peptides for fibronectin binding integrin subtypes α5β1 and αvβ6: Conformational control through flanking amino acids. *J. Med. Chem.* **2013**, *56*, 1509–1519.

[24] Curnis, F.; Sacchi, A.; Longhi, R.; Colombo, B.; Gasparri, A.; Corti, A. IsoDGR-tagged albumin: A new αvβ3 selective carrier for nanodrug delivery to tumors. *Small* **2013**, *9*, 673–678.

[25] Curnis, F.; Corti, A. Production and characterization of recombinant human and murine TNF. *Methods Mol. Med.* **2004**, *98*, 9–22.

[26] Dondossola, E.; Rangel, R.; Guzman-Rojas, L.; Barbu, E. M.; Hosoya, H.; St John, L. S.; Molldrem, J. J.; Corti, A.; Sidman, R. L.; Arap, W. et al. CD13-positive bone marrow-derived myeloid cells promote angiogenesis, tumor growth, and metastasis. *Proc. Natl. Acad. Sci. USA* **2013**, *110*, 20717–20722.

[27] Wong, A. H. M.; Zhou, D. X.; Rini, J. M. The X-ray crystal structure of human aminopeptidase N reveals a novel dimer and the basis for peptide processing. *J. Biol. Chem.* **2012**, *287*, 36804–36813.

[28] Merlot, A. M.; Kalinowski, D. S.; Richardson, D. R. Unraveling the mysteries of serum albumin-more than just a serum protein. *Front. Physiol.* **2014**, *5*, 299.

[29] Colombo, G.; Curnis, F.; De Mori, G. M. S.; Gasparri, A.; Longoni, C.; Sacchi, A.; Longhi, R.; Corti, A. Structure-activity relationships of linear and cyclic peptides containing the NGR tumor-homing motif. *J. Biol. Chem.* **2002**, *277*, 47891–47897.

[30] Liu, C.; Yang, Y.; Chen, L.; Lin, Y. L.; Li, F. A unified mechanism for aminopeptidase N-based tumor cell motility and tumor-homing therapy. *J. Biol. Chem.* **2014**, *289*, 34520–34529.

[31] Fields, G. B.; Noble, R. L. Solid phase peptide synthesis utilizing 9-fluorenylmethoxycarbonyl amino acids. *Int. J. Pept. Protein Res.* **1990**, *35*, 161–214.